Supplementary Material
Interfering tunneling paths through magnetic molecules on superconductors: Asymmetries of Kondo and Yu-Shiba-Rusinov resonances

Laëtitia Farinacci,[1] Gelavizh Ahmadi,[1] Michael Ruby,[1] Gaël Reecht,[1] Benjamin W. Heinrich,[1] Constantin Czekelius,[2] Felix von Oppen,[3] and Katharina J. Franke[1]

[1] *Fachbereich Physik, Freie Universität Berlin, Arnimallee 14, 14195 Berlin, Germany*
[2] *Institut für Organische Chemie und Makromolekulare Chemie, Heinrich-Heine-Universität Düsseldorf, 40225 Düsseldorf, Germany*
[3] *Dahlem Center for Complex Quantum Systems and Fachbereich Physik, Freie Universität Berlin, 14195 Berlin, Germany*

(Dated: October 10, 2020)

EXPERIMENTAL DETAILS AND ADDITIONAL DATA

Experimental details

The Pb(111) substrate was cleaned by sputtering with Ne^+ ions at 0.9 kV under ultra-high vacuum conditions. Annealing the sample at 430 K leads to atomically flat and clean terraces. FeTPyP-Cl molecules were deposited from a Knudsen cell at 673 K while the Pb sample was kept at 313 K. The as-prepared sample was cooled down and transferred into the Joule-Thomson STM (by Specs). All experiments were carried out at a temperature of 1.1 K.

We used Pb-covered tips for all data shown in the main manuscript and SM. These were prepared by indenting the tip into the clean Pb substrate while applying a voltage of $V = 100$ V. Their spectroscopic properties were tested on the bare Pb(111) substrate. The indentation procedure was repeated until the tip developed a bulk-like superconducting Bardeen-Cooper-Schrieffer (BCS) energy gap of $\Delta_{\mathrm{tip}} = 1.35$ meV. Such a tip is of amorphous nature and exhibits a single gap, whereas the single-crystal substrate reveals the two-band superconducting properties pf Pb and exhibits two distinct BCS gaps with $\Delta_1 = 1.30$ meV and $\Delta_2 = 1.44$ meV [1]. The sharp coherence peaks in the tip allow for an effective energy resolution beyond the thermal Fermi-Dirac limit. In essence, the superconducting gap of the tip leads to a shift of all sample features by Δ_{tip}. As the tip's quasi-particle density of states is symmetric in intensity around the Fermi level, the tip does not modify any asymmetries in the spectral properties of the sample.

Differential conductance spectra were recorded using an external lock-in amplifier with a modulation frequency of $f = 911$ Hz. The modulation amplitudes are given in the corresponding figure captions.

We use different feedback control methods for recording $\mathrm{d}I/\mathrm{d}V$ maps. In the "constant-contour" mode, often also referred to as "multi-pass", we first record a constant-current image with certain feedback parameters. These determine the height profile of the tip across the surface. This profile is subsequently used for scanning along the same path with the desired bias voltage while recording the $\mathrm{d}I/\mathrm{d}V$ signal. The data is exactly the same (but much faster in its acquisition) as the $\mathrm{d}I/\mathrm{d}V$ values extracted from a densely spaced grid of spectra recorded when opening the feedback at the set contour value. Figs. 2d,e have been acquired with this method.

A bias voltage of 5 mV was chosen when opening the feedback loop for the acquisition of all spectra in Fig. 1. A small bias voltage is ideal as it ensures that only a small range of electronic states contributes to the tunneling current. However, in the case of FeTPyP on Pb(111), the highest occupied molecular orbital (HOMO) extends across the Fermi level and we observe a non-negligible contribution to the tunneling current. Hence, the image is not only of topographic origin, but convolved with these states. For this reason, the STM image (Fig. 1b) does not only show the tilted pyridine legs, which are expected to be highest in topography [2], but also the three lobes of the HOMO resonance along the pyrrole saddle.

To map the iso-density of a particular orbital, the method of choice is to use the $\mathrm{d}I/\mathrm{d}V$ signal itself for feedback control [3]. This procedure has been employed for the acquisition of the maps in Fig. 3b.

Evolution of Kondo and YSR asymmetry along an FeTPyP molecule

In the main text, we show three representative spectra of the Kondo resonance and the YSR states measured along the pyrrole saddle of FeTPyP. In Fig. S1b,c, we show color plots of a series of densely spaced spectra, taken along the same line, for the Kondo and YSR states, respectively. These spectra were used to extract the asymmetry shown in Fig. 1e,f in the manuscript.

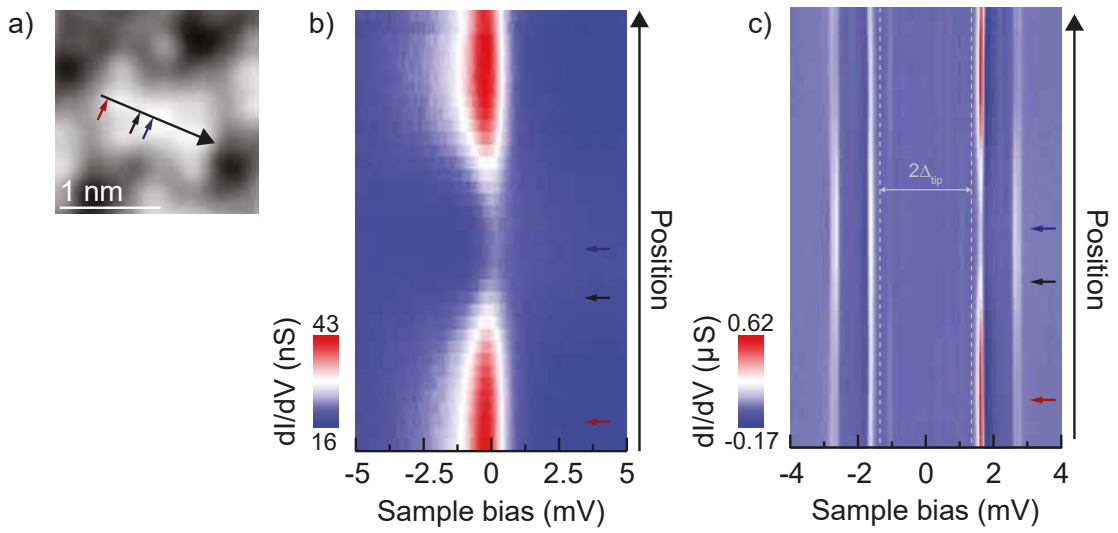

Figure S1. (a) Topography image of one molecule (same as in Fig. 1b) with an arrow indicating the line along which a set of Kondo and YSR spectra have been recorded ($V = 5\,\mathrm{mV}$, $I = 100\,\mathrm{pA}$). The colored arrows mark the positions of the spectra in Fig. 1 and are also used as markers in (b,c). (b) Color plot of $\mathrm{d}I/\mathrm{d}V$ spectra of the Kondo resonance measured in an external magnetic field of $B = 1.5\,\mathrm{T}$ to quench superconductivity in substrate and tip (feedback opened at $V = 5\,\mathrm{mV}$, $I = 100\,\mathrm{pA}$ and signal modulated with $V_{\mathrm{rms}} = 100\,\mu\mathrm{eV}$). These spectra have been used to extract the asymmetry shown in Fig. 1e. (c) $\mathrm{d}I/\mathrm{d}V$ spectra recorded with a superconducting tip and substrate in the absence of the B-field (feedback opened at $V = 5\,\mathrm{mV}$, $I = 100\,\mathrm{pA}$ and signal modulated with $V_{\mathrm{rms}} = 15\,\mu\mathrm{eV}$). The superconducting energy gap of the tip is indicated by dashed lines. The YSR states appear as a pair of resonances symmetric in energy around the Fermi level, but asymmetric in intensity. These spectra have been used to extract the asymmetry shown in Fig. 1f.

Magnetic field dependence of Kondo resonance

To quench the superconducting state of substrate and tip, we applied an external magnetic field of $B = 1.5\,\mathrm{T}$ perpendicular to the surface. The evolution of the Kondo resonance with increasing field strength is shown in Fig. S2. At 3 T we observe a clear splitting of the Kondo resonance, which can be reproduced by two Fano-Frota functions shifted by $\pm 450\mu\mathrm{eV}$ from the Fermi level. The observed splitting is larger than the $\pm 350\mu\mathrm{eV}$ energy splitting expected for a spin $S = 1/2$. We attribute this behavior to an underscreened $S = 1$ Kondo system [4]. However, we note that our temperature and modulation broadening of $\sqrt{(2V_{\mathrm{rms}}^2) + (3.5k_BT)^2} = 390\ \mu\mathrm{eV}$ is of the same order of magnitude, preventing a clear assignment of the splitting.

We also note that at a field strength of 1.5 T, we do not observe a splitting of the Kondo resonance, because the thermal broadening is still much larger than the expected splitting. This justifies the fit with a single Fano-Frota function.

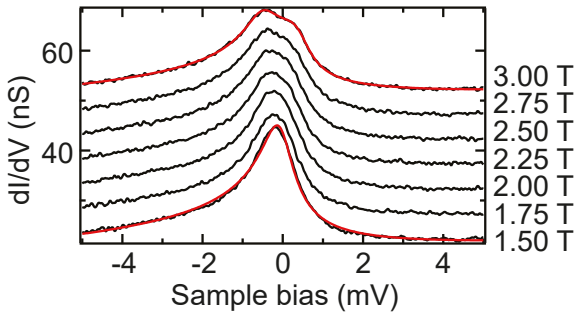

Figure S2. $\mathrm{d}I/\mathrm{d}V$ spectra showing the evolution of the Kondo resonance with increasing magnetic field strength (feedback opened at $V = 5\,\mathrm{mV}$, $I = 100\,\mathrm{pA}$, modulation voltage $V_{\mathrm{rms}} = 100\ \mu\mathrm{eV}$). The spectra are offset for clarity. Red lines are fits with one (at 1.5 T) and two (at 3 T) Fano-Frota functions.

Identification of YSR coupling regime

The observation of a pair of YSR states reveals the exchange coupling to the substrate. However, this does not allow for the identification of the many-body ground state, i.e., for the assignment of the screened or unscreened spin state of the FeTPyP molecule (singlet and doublet many-body ground states, respectively). By approaching the STM tip toward the molecule, the attractive potential of the tip lifts the molecule from the substrate. Hence, we can investigate the shift of the YSR state with the associated decrease in the exchange coupling strength [5]. Figure S3 reveals that the YSR states move towards the superconducting gap edge upon tip approach. This behavior shows that the molecule is in the unscreened regime. The narrow Kondo linewidth is in agreement with this assignment [6].

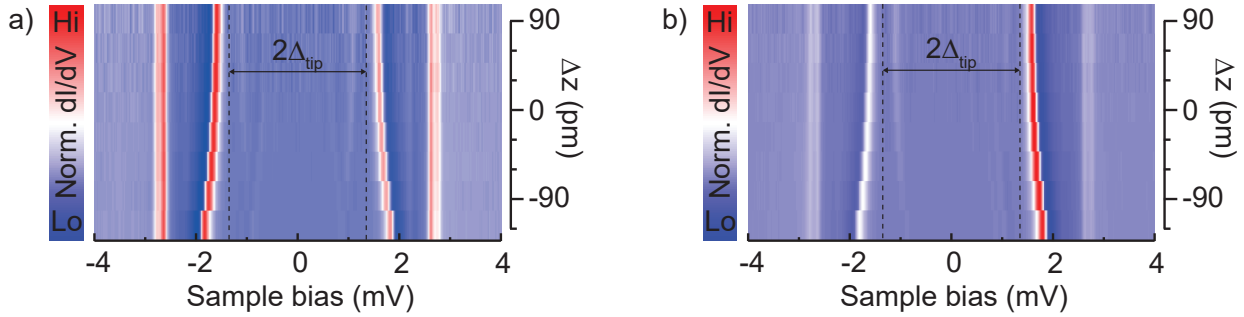

Figure S3. Normalized dI/dVspectra upon tip approach on (a) the Fe center and (b) upper pyrrole (feedback opened at $V = 5\,\mathrm{mV}$, $I = 100\,\mathrm{pA}$, and subsequent variation of tip height z, modulation voltage $V_{\mathrm{rms}} = 15\ \mu\mathrm{eV}$. The superconducting energy gap of the tip is indicated by dashed lines. The YSR states shift toward the superconducting gap edge upon tip approach, indicating that the FeTPyP molecule lies in the unscreened spin regime.

THEORETICAL CONSIDERATIONS

Model

We start by considering the spin state of Fe in FeTPyP. With the central Cl ligand detached, the molecule presumably is in oxidation state +2 and its square-planar ligand field splits the Fe d-shell into four sets. For an unoccupied topmost $d_{x^2-y^2}$ orbital, this results in a $S = 1$ spin state. In order of ascending energy, one expects a doubly-occupied d_{xy} orbital, degenerate d_{xz} and d_{yz} orbitals occupied by three electrons, and a singly-occupied d_{z^2} orbital. The d orbitals are hybridized with the orbitals of the organic ligand, resulting in an extended spin-carrying orbital. Due to the largest overlap with the substrate, we expect the d_{z^2}-derived orbital to give rise to the Kondo effect, with the two unpaired electrons being Hund coupled [7]. This picture is consistent with the observed spin splitting of the Kondo resonance in a magnetic field (see Fig. S2) and with the observation of only a single Kondo temperature T_K, irrespective of tip location. We also identify only a single Yu-Shiba-Rusinov (YSR) state. In particular, there is no evidence for a second YSR state which splits off from the YSR peak or superconducting gap edge upon tip approach. These observations are consistent with an underscreened Kondo effect, in which the $S = 1$ impurity spin is screened by a single channel of substrate electrons.

The scanning-tunneling-microscopy (STM) data suggest that a second orbital (or even several orbitals) are involved in determining the low-bias tunneling spectra, both with and without superconductivity. In particular, there may be one or several resonances beginning at $V = -360\,\mathrm{mV}$ which weakly overlap with the Fermi energy (see Fig. 3a of the main text) and thus constitute a second tunneling channel. We refer to this (set of) resonance(s) as the HOMO. Mapping out this molecular orbital structure reveals nodal planes (see Fig. 3b of the main text) where the wavefunction changes sign. A central ingredient of our model is that tip-substrate tunneling via this second orbital includes a substantial potential-scattering amplitude. To bring out the essential physics, we will discuss our model in the following for the case that the HOMO is nonmagnetic in nature and contributes potential scattering only between tip and substrate. It should be understood, however, that this is not a necessary assumption for our model to explain the experimental results. If the HOMO is also magnetic, we merely have to assume that it does not develop strong Kondo correlations (as indeed suggested by the data which exhibit only a single Kondo temperature). In the absence of strong Kondo correlations, the exchange coupling has not yet flown to strong coupling at the relevant energy

scales (as set by temperature and the superconducting gap) and tunneling between tip and substrate via the HOMO can include a substantial potential scattering amplitude in addition to the exchange-scattering contribution. In this situation, one finds qualitatively the same results as in the reduced model discussed below. In particular, we note that the exchange scattering amplitude contributed by tunneling via a magnetic HOMO would also change sign at the nodal plane so that the coincidence of symmetric Kondo and YSR peaks with the nodal plane is still be expected from such a modified model.

As a minimal model, we thus consider two molecular orbitals: (i) a singly-occupied orbital which derives from the Fe d orbitals (but has nonzero amplitude both on the Fe center and the ligand as a result of hybridization) and develops a magnetic moment due to an onsite interaction U, and (ii) a doubly-occupied orbital which represents the HOMO and has negligible onsite interaction. The annihilation operator for an electron of spin σ in the first, spin-carrying orbital of energy ϵ_d is denoted by d_σ. We perform a particle-hole transformation for the second (HOMO) orbital, resulting in a hole orbital of energy ϵ_h and hole-annihilation operator h_σ. (In the following, the hole nature of this orbital will be left implicit.) Then, the Hamiltonian becomes

$$\begin{aligned} H = &\sum_{\mathbf{k}\sigma} \epsilon_{L\mathbf{k}} \psi^\dagger_{L\mathbf{k}\sigma} \psi_{L\mathbf{k}\sigma} + \sum_{\mathbf{k}\sigma} \epsilon_{R\mathbf{k}} \psi^\dagger_{R\mathbf{k}\sigma} \psi_{R\mathbf{k}\sigma} + \sum_\sigma \epsilon_h h^\dagger_\sigma h_\sigma + \sum_\sigma \epsilon_d d^\dagger_\sigma d_\sigma + U d^\dagger_\uparrow d^\dagger_\downarrow d_\downarrow d_\uparrow \\ &+ \sum_\sigma \left[t_{Lh} h^\dagger_\sigma \psi_{L\sigma}(\mathbf{0}) + t_{Ld} d^\dagger_\sigma \psi_{L\sigma}(\mathbf{0}) + t_{Rh} \psi^\dagger_{R\sigma}(\mathbf{0}) h_\sigma + t_{Rd} \psi^\dagger_{R\sigma}(\mathbf{0}) d_\sigma + \text{h.c.} \right] \end{aligned} \tag{S1}$$

Here, electrons of wavevector $\mathbf{k}$ in tip and substrate are annihilated by $\psi_{L\mathbf{k}\sigma}$ and $\psi_{R\mathbf{k}\sigma}$, respectively. The operators $\psi_{L\sigma}(\mathbf{0})$ and $\psi_{R\sigma}(\mathbf{0})$ annihilate electrons in tip and substrate at the location of the tunnel junction to the molecular adsorbate. For the tip, the origin $\mathbf{0}$ is measured relative to a coordinate system attached to the tip.

The tunneling matrix elements t_{Lh} and t_{Ld} between tip and molecule depend on the position $\mathbf{R}$ of the tip relative to the molecule, and reflect the wavefunctions of the molecular orbitals. In particular, $t_{Lh}(\mathbf{R})$ changes sign at the nodal planes of the HOMO. There is no evidence in the data for nodal planes in the spin-carrying orbitals, so that we assume that $t_{Ld}(\mathbf{R})$ has a fixed sign. The tunneling amplitudes t_{Rh} and t_{Rd} between molecule and substrate are independent of tip position and fixed by the adsorption geometry of the molecule on the substrate. We finally note that the tunneling amplitudes t_{Lh}, t_{Ld}, t_{Rh}, and t_{Rd} can be chosen as real by time reversal symmetry.

Kondo resonance

Fano lineshape of Kondo resonance

Fano lineshapes emerge from the interference of a resonant channel with a rapid dependence of the scattering amplitude on energy and a nonresonant channel for which the energy dependence can be neglected on the scale of the broadening of the resonance. In the context of adatom experiments, the nonresonant channel is frequently identified with direct tunneling into the substrate which then interferes with a resonant scattering channel via the adatom which results from the Kondo effect [8, 9]. For molecular adsorbates, tunneling between tip and substrate is presumably mediated by molecular orbitals as long as the tip is positioned above the molecule [10]. In keeping with the model Hamiltonian in Eq. (S1), we therefore neglect direct tunneling between tip and substrate and show that the Fano lineshape is naturally explained by interference between tunneling paths associated with two molecular orbitals. A recent study argued that similar processes are also relevant for Kondo resonances induced by magnetic adatoms [11].

Assuming weak tunneling between tip and molecular adsorbate, the differential conductance can be written as

$$\frac{\mathrm{d}I}{\mathrm{d}V} = \frac{2e^2}{h} 2\pi \nu_L \rho_{rr^\dagger}(eV), \tag{S2}$$

where ν_L is the electronic density of states of the tip and $\rho_{rr^\dagger}(\omega)$ denotes the relevant spectral function of the substrate,

$$\rho_{rr^\dagger}(\omega) = -2\mathrm{Im} G_{rr^\dagger}(\omega + i\eta) \tag{S3}$$

(η denotes a positive infinitesimal) with

$$r^\dagger = t_{Lh} h^\dagger + t_{Ld} d^\dagger \tag{S4}$$

and $G_{rr^\dagger}(\omega + i\eta)$ denoting the Fourier transform of the retarded Green function

$$G_{rr^\dagger}(t, t') = -i\theta(t - t') \langle [r(t), r^\dagger(t')] \rangle. \tag{S5}$$

Since the spectral function is proportional to a unit matrix in spin space, we have dropped spin indices. We can then write

$$\frac{\mathrm{d}I}{\mathrm{d}V} = \frac{2e^2}{h} 4\pi^2 \nu_L \frac{-1}{\pi} \mathrm{Im}\left\{ t_{Lh} G_{hh^\dagger}(eV) t_{Lh} + t_{Lh} G_{hd^\dagger}(eV) t_{Ld} + t_{Ld} G_{dh^\dagger}(eV) t_{Lh} + t_{Ld} G_{dd^\dagger}(eV) t_{Ld} \right\}, \tag{S6}$$

where the Green functions are defined by analogy with Eq. (S5) and the positive infinitesimal is left implicit.

As a consequence of the Kondo effect, the Green function $G_{dd^\dagger}(\omega + i\eta)$ of the spin-carrying orbital exhibits a sharp resonance at the Fermi energy. We therefore relate the remaining Green functions in Eq. (S6) to $G_{dd^\dagger}(\omega + i\eta)$. This yields (see Ref. [9] for a similar expression in the case that the parallel channel originates from direct tunneling into the substrate)

$$\begin{aligned}\frac{\mathrm{d}I}{\mathrm{d}V} = \frac{2e^2}{h} 4\pi^2 \nu_L \frac{-1}{\pi} \mathrm{Im}\{ & t_{Lh} \tilde{g}_{hh^\dagger}(eV) t_{Lh} \\ & + [t_{Ld} + t_{Lh} \tilde{g}_{hh^\dagger}(eV) t_{Rh} g_{RR^\dagger}(eV) t_{Rd}] G_{dd^\dagger}(eV) [t_{Ld} + t_{Rd} g_{RR^\dagger}(eV) t_{Rh} \tilde{g}_{hh^\dagger}(eV) t_{Lh}] \}. \end{aligned} \tag{S7}$$

Here, a capital G denotes a fully dressed Green function, a lower-case g denotes a bare Green function (g) or a Green function including a subset of self-energy contributions ($\tilde{g}$). We sketch the derivation of Eq. (S7) in the subsequent section. Since it can also be readily understood physically, we proceed first with a qualitative justification and focus on how it predicts a Fano lineshape for the Kondo resonance. The first term within the curly brackets describes tunneling from tip to substrate via the HOMO in the absence of the d orbital. Correspondingly, this term involves the Green function

$$\tilde{g}_{hh^\dagger}(\omega) = \frac{1}{\omega - \epsilon_h - t_{Rh} g_{RR^\dagger}(\omega) t_{Rh}} = \frac{1}{\omega - \epsilon_h + i\pi (t_{Rh})^2 \nu_R} \tag{S8}$$

of the HOMO including the self energy correction due to tunneling into the bare substrate. The latter enters through the Green function $g_{RR^\dagger}(\omega)$ of the bare substrate in the absence of the molecular adsorbate. Neglecting the spatial extent of the molecule for simplicity, this Green function enters only with equal spatial indices of its two electron operators, and we have

$$g_{RR^\dagger}(\omega) = -i\pi\nu_R \tag{S9}$$

in terms of the electronic density of states ν_R of the bare substrate. The second term in the curly bracket collects all contributions which proceed via the d orbital and are thus sensitive to the Kondo resonance. The contribution involving t_{Ld}^2 describes direct tunneling from the tip into the d orbital, dressed by its coupling to the remainder of the system. Similarly, the term proportional to t_{Lh}^2 describes a process in which an electron tunnels from the tip into the dressed d orbital via a multistep process involving the HOMO and the substrate. Finally, the terms involving $t_{Ld} t_{Lh}$ describe contributions which arise from interference of the previous two tunneling paths.

To bring out the essential physics of the Fano lineshape, we note that the two terms in square brackets in Eq. (S7) are identical and complex. Defining the polar representation

$$\sqrt{\mathcal{A}} e^{i\phi/2} = t_d + t_{Lh} \tilde{g}_{hh^\dagger}(eV) t_{Rh} g_{RR^\dagger}(eV) t_{Rd}, \tag{S10}$$

Eq. (S7) becomes

$$\frac{\mathrm{d}I}{\mathrm{d}V} = \frac{2e^2}{h} 4\pi^2 \nu_L \frac{-1}{\pi} \mathrm{Im}\left\{ t_{Lh} \tilde{g}_{hh^\dagger}(eV) t_{Lh} + \mathcal{A} e^{i\phi} G_{dd^\dagger}(eV) \right\}. \tag{S11}$$

We evaluate Eqs. (S10) and (S11) by keeping only the leading nonvanishing contributions of $\tilde{g}_{hh^\dagger}(\omega)$ in the limit in which the broadening of the HOMO is small compared to its energy ϵ_h measured from the Fermi energy. (It should be evident that it is straight-forward to go beyond this approximation, but this is unnecessary for our purposes.) With this approximation, $\tilde{g}_{hh^\dagger}(eV) \simeq -i\pi (t_{Rh})^2 \nu_R / \epsilon_h^2$ in the first term in curly bracket in Eq. (S11) and $\tilde{g}_{hh^\dagger}(eV) \simeq -1/\epsilon_h$ in Eq. (S10). This yields

$$\sqrt{\mathcal{A}} e^{i\phi/2} = t_d + i\pi \frac{t_{Lh} t_{Rh}}{\epsilon_h} \nu_R t_{Rd}. \tag{S12}$$

Since the imaginary part of the right-hand side is proportional to the tunneling amplitude t_{Lh} into the HOMO of the molecule, the phase ϕ passes through zero and changes sign at the nodal plane.

Within a simple, but useful approximation, we can express the d-orbital Green function in the vicinity of the Fermi energy as [12]

$$G_{dd^\dagger}(eV) = \frac{Z_K}{eV - \epsilon_K + iT_K}, \tag{S13}$$

where Z_K denotes the intrinsic strength of the Kondo resonance, $\epsilon_K \simeq 0$ its energy, and T_K the Kondo temperature. The shape of the Kondo resonance is frequently fitted more accurately by the Frota function [13]

$$G_{dd^\dagger}(eV) = \frac{-iZ_K}{T_K}\sqrt{\frac{iT_K}{eV - \epsilon_K + iT_K}}. \tag{S14}$$

Inserting this expression into Eq. (S11), we obtain

$$\left.\frac{\mathrm{d}I}{\mathrm{d}V}\right|_{\mathrm{res}} = \frac{2e^2}{h} 4\pi^2 \nu_L \mathrm{Re}\left\{\mathcal{A}e^{i\phi}\frac{Z_K}{\pi T_K}\sqrt{\frac{iT_K}{eV - \epsilon_K + iT_K}}\right\}. \tag{S15}$$

This expression has the same form as Eq. (1) of the main text. It also shows that the sign change of the HOMO wavefunction changes the sense of asymmetry of the Kondo resonance, as we observe experimentally.

Green-function expression (S7)

In this section, we sketch the derivation of Eq. (S7) from Eq. (S6). This requires one to relate the various Green functions entering Eq. (S6) to $G_{dd^\dagger}$. Since interactions enter only on the d orbital, this can be done with the help of the equations of motions of the Green functions. One readily finds the Dyson equations

$$G_{hh^\dagger} = g_{hh^\dagger} + g_{hh^\dagger} t_{Rh} G_{Rh^\dagger} \tag{S16}$$
$$G_{hR^\dagger} = g_{hh^\dagger} t_{Rh} G_{RR^\dagger} \tag{S17}$$
$$G_{hd^\dagger} = g_{hh^\dagger} t_{Rh} G_{Rd^\dagger} \tag{S18}$$
$$G_{Rh^\dagger} = g_{RR^\dagger} t_{Rh} G_{hh^\dagger} + g_{RR^\dagger} t_{Rd} G_{dh^\dagger} \tag{S19}$$
$$G_{RR^\dagger} = g_{RR^\dagger} + g_{RR^\dagger} t_{Rh} G_{hR^\dagger} + g_{RR^\dagger} t_{Rd} G_{dR^\dagger} \tag{S20}$$
$$G_{Rd^\dagger} = g_{RR^\dagger} t_{Rh} G_{hd^\dagger} + g_{RR^\dagger} t_{Rd} G_{dd^\dagger} \tag{S21}$$
$$G_{Rh^\dagger} = G_{RR^\dagger} t_{Rh} g_{hh^\dagger} \tag{S22}$$
$$G_{dh^\dagger} = G_{dR^\dagger} t_{Rh} g_{hh^\dagger} \tag{S23}$$
$$G_{dR^\dagger} = G_{dh^\dagger} t_{Rh} g_{RR^\dagger} + G_{dd^\dagger} t_{Rd} g_{RR^\dagger}. \tag{S24}$$

Here, $g_{hh^\dagger}(\omega) = 1/(\omega - \epsilon_h + i\eta)$ denotes the Green function of the uncoupled HOMO. The first six expressions result from equations of motions involving time derivatives with respects to the first time argument of the Green function. The last three identities follow from equations of motions with respect to the second time argument.

We first insert Eq. (S24) into Eq. (S23) and solve for $G_{dh^\dagger}$. This yields

$$G_{dh^\dagger} = G_{dd^\dagger} t_{Rd} g_{RR^\dagger} t_{Rh} g_{hh^\dagger} \frac{1}{1 - t_{Rh} g_{RR^\dagger} t_{Rh} g_{hh^\dagger}} \tag{S25}$$

and thus

$$G_{dh^\dagger} = G_{dd^\dagger} t_{Rd} g_{RR^\dagger} t_{Rh} \tilde{g}_{hh^\dagger}. \tag{S26}$$

Similarly, inserting Eq. (S21) into Eq. (S18) and solving for $G_{hd^\dagger}$, we find

$$G_{hd^\dagger} = \frac{1}{1 - g_{hh^\dagger} t_{Rh} g_{RR^\dagger} t_{Rh}} g_{hh^\dagger} t_{Rh} g_{RR^\dagger} t_{Rd} G_{dd^\dagger} \tag{S27}$$

and thus

$$G_{hd^\dagger} = \tilde{g}_{hh^\dagger} t_{Rh} g_{RR^\dagger} t_{Rd} G_{dd^\dagger}. \tag{S28}$$

Finally, we insert Eq. (S19) into Eq. (S16) and solve for $G_{hh^\dagger}$. This yields

$$G_{hh^\dagger} = \frac{1}{1 - g_{hh^\dagger} t_{Rh} g_{RR^\dagger} t_{Rh}} g_{hh^\dagger} (1 + t_{Rh} g_{RR^\dagger} t_{Rd} G_{dh^\dagger}) \tag{S29}$$

and thus

$$G_{hh^\dagger} = \tilde{g}_{hh^\dagger} + \tilde{g}_{hh^\dagger} t_{Rh} g_{RR^\dagger} t_{Rd} G_{dh^\dagger}. \tag{S30}$$

Inserting Eq. (S26), we obtain

$$G_{hh^\dagger} = \tilde{g}_{hh^\dagger} + \tilde{g}_{hh^\dagger} t_{Rh} g_{RR^\dagger} t_{Rd} G_{dd^\dagger} t_{Rd} g_{RR^\dagger} t_{Rh} \tilde{g}_{hh^\dagger}. \tag{S31}$$

We can now insert Eqs. (S26), (S28), and (S31) into Eq. (S6) and obtain Eq. (S7).

YSR resonances

Schrieffer-Wolff transformation

To understand the asymmetry of the YSR resonances at positive and negative bias voltages, it is convenient to eliminate the spin-carrying d orbital as well as the HOMO by a Schrieffer-Wolff transformation and to obtain an effective low-energy Hamiltonian.

The molecular d orbital leads to exchange and potential scattering terms,

$$H_d = \sum_{\alpha\alpha'} J^{(d)}_{\alpha\alpha'}(\mathbf{R}) \mathbf{S} \cdot \psi^\dagger_\alpha(\mathbf{0}) \boldsymbol{\sigma} \psi_{\alpha'}(\mathbf{0}) + \sum_{\alpha\alpha'} V^{(d)}_{\alpha\alpha'}(\mathbf{R}) \psi^\dagger_\alpha(\mathbf{0}) \psi_{\alpha'}(\mathbf{0}) \tag{S32}$$

with the impurity-spin operator $\mathbf{S}$, the vector $\boldsymbol{\sigma}$ of Pauli matrices, and the spinor of electron field operators $\psi_\alpha(\mathbf{0}) = [\psi_{\alpha,\uparrow}(\mathbf{0}), \psi_{\alpha,\downarrow}(\mathbf{0})]^T$ in the tip ($\alpha = L$) and the substrate ($\alpha = R$; with $\mathbf{0}$ denoting the adsorption position of the molecule). In contrast, the nonmagnetic HOMO gives rise to a potential scattering term only,

$$H_h = \sum_{\alpha\alpha'} V^{(h)}_{\alpha\alpha'}(\mathbf{R}) \psi^\dagger_\alpha(\mathbf{0}) \psi_{\alpha'}(\mathbf{0}). \tag{S33}$$

The Schrieffer-Wolff transformation yields

$$J^{(d)}_{\alpha\alpha'}(\mathbf{R}) = t_{\alpha d} t^*_{\alpha' d} \left[\frac{1}{\epsilon_d + U} - \frac{1}{\epsilon_d} \right] \tag{S34}$$

for the exchange coupling and

$$V^{(d)}_{\alpha\alpha'}(\mathbf{R}) = t_{\alpha d} t^*_{\alpha' d} \left[\frac{1}{\epsilon_d + U} + \frac{1}{\epsilon_d} \right] \tag{S35}$$

for the amplitude of potential scattering from the molecular d orbital. Similarly, the HOMO results in the amplitude

$$V^{(h)}_{\alpha\alpha'}(\mathbf{R}) = t_{\alpha h} t^*_{\alpha' h} \frac{1}{\epsilon_h} \tag{S36}$$

of potential scattering.

In experiment, the tip-molecule coupling is much weaker than the molecule-substrate coupling. We thus neglect the exchange and potential-scattering processes which only involve the tip (i.e., we set $J^{(d)}_{LL} = V^{(d)}_{LL} = V^{(h)}_{LL} = 0$) and treat terms which scatter electrons between tip and substrate perturbatively. In leading order, the molecule is then coupled to the substrate through $J^{(d)}_{RR}$ and $V^{(d)}_{RR}$ as well as $V^{(h)}_{RR}$. The strong Kondo correlations arise as the exchange coupling flows to strong coupling at low energies, and we can thus neglect $V^{(d/h)}_{RR}$ relative to $J^{(d)}_{RR}$ in discussing low-bias tunneling. For the same reason, scattering between tip and substrate via the spin-carrying orbital is dominated by the exchange term, and we neglect $V^{(d)}_{RL}$ and $V^{(d)}_{LR}$.

As a result of these considerations, we obtain the effective Hamiltonian

$$H = H_0 + H_1 \tag{S37}$$

with unperturbed Hamiltonian

$$H_0 = \sum_\alpha H_\alpha + J^{(\mathrm{d})}_{RR}(\mathbf{R})\mathbf{S}\cdot\psi^\dagger_R(\mathbf{0})\boldsymbol{\sigma}\psi_R(\mathbf{0}). \tag{S38}$$

and tunneling perturbation

$$H_1 = \psi^\dagger_R(\mathbf{0})\left[J^{(\mathrm{d})}_{RL}(\mathbf{R})\mathbf{S}\cdot\boldsymbol{\sigma} + V^{(\mathrm{h})}_{RL}(\mathbf{R})\right]\psi_L(\mathbf{0}) + \mathrm{h.c.}. \tag{S39}$$

As time-reversal symmetry implies that all tunneling amplitudes can be chosen real, this also holds true for $J^{(\mathrm{d})}_{\alpha\alpha'}(\mathbf{R})$ and $V^{(\mathrm{h})}_{\alpha\alpha'}(\mathbf{R})$. The Kondo correlations as well as the YSR states are induced by the exchange coupling between molecular spin $\mathbf{S}$ and substrate included in H_0. Tunneling between tip and substrate proceeds via two separate channels involving the molecular d orbital and the HOMO, respectively. While the second tunneling channel is independent of electron spin, the first is spin dependent. According to Eq. (S36), the sign change of the HOMO wavefunction at the nodal plane introduces a sign change of the potential scattering amplitude $V^{(h)}(\mathbf{R})$.

Asymmetry of YSR resonances

We now derive the tunneling current into the YSR state by Fermi's golden rule. At large tip distances, tunneling between tip and substrate is rate limited by the tunneling between tip and YSR state [14]. The resulting subgap excitation (i.e., a quasiparticle occupying the YSR state) relaxes into the quasiparticle continuum by inelastic processes which are more frequent than tunneling. As a consequence of the strong Kondo correlations, the YSR state originates from strong exchange coupling J_{RR} between molecular orbital and substrate, with potential scattering V_{RR} being a small perturbation. In this case, one expects that the electron and hole wavefunctions of the YSR states are approximately equal. For instance, it is well known that the asymmetry between electron and hole wavefunctions is due to nonzero potential scattering when modeling the impurity as a classical spin.

Motivated by the experiment, we assume that the YSR state is on the weak-coupling (unscreened) side of the quantum phase transition between doublet (unscreened) and singlet (screened) ground states. (As mentioned in the main text, this assumption is made for definiteness. Our conclusions would not change for a YSR state in the strong-coupling state and the following arguments can be readily adapted to this case.) In this case, the substrate superconductor is in a fully paired ground state $|\mathrm{even}\rangle$ with even fermion parity, and tunneling is into the excited odd-fermion parity state $|\mathrm{odd}\rangle = \gamma^\dagger_\epsilon|\mathrm{even}\rangle$ with a quasiparticle occupying the YSR state (with Bogoliubov operator γ_ϵ). For simplicity, we assume a classical-spin model for the impurity in the following, i.e., we effectively keep only the exchange coupling to S_z. This suffices to elucidate the emergence of the asymmetry between the bias directions due to the presence of two parallel tunneling channels. As this asymmetry is clearly associated with the different behaviors of exchange and potential scattering under time reversal of the substrate Hamiltonian (for a given impurity spin), the underlying mechanism is expected to be robust when extending the theory to include the full quantum nature of the impurity spin. Developing such a theory would be an interesting problem for future research, but is beyond the scope of the present paper.

To compute the tunneling rate between superconducting tip and substrate, we expand the electron operator of the substrate into Bogoliubov operators. At subgap bias voltages, we only need to retain the contribution of the YSR state. We take the impurity spin as polarized in the positive z-direction, so that the YSR bound state is polarized along the negative z-direction. We can then write the substrate electron operators as

$$\psi_{R,\downarrow}(\mathbf{r}) = u_\epsilon(\mathbf{r})\gamma_\epsilon + \ldots \tag{S40}$$

and

$$\psi_{R,\uparrow}(\mathbf{r}) = -v^*_\epsilon(\mathbf{r})\gamma^\dagger_\epsilon + \ldots, \tag{S41}$$

with the ellipses referring to the contributions of above-gap quasiparticles. Here, we have introduced the electron and hole wavefunctions $u_\epsilon(\mathbf{r})$ and $v_\epsilon(\mathbf{r})$ of the YSR state. These equations reflect that due to the spin polarization of the YSR state, removing a quasiparticle is associated with annihilating a down-spin electron. Conversely, removing an up-spin electron from the ground state necessarily breaks a Cooper pair and its spin-down electron can subsequently occupy the YSR state.

First consider tunneling from the tip into the YSR state of energy ϵ_s at positive bias voltages. Fermi's golden rule gives the tunnel current

$$I|_+ = \frac{2\pi e}{\hbar}\sum_{\mathbf{k},\sigma}|\langle \text{odd}; E_{Lk}|H_1|\text{even}; \text{BCS}_L\rangle|^2\delta(eV - E_{Lk} - \epsilon_s), \tag{S42}$$

where $|\text{BCS}_L\rangle$ and $|E_{Lk}\rangle$ denote the BCS ground state and a state with a single Bogoliubov quasiparticle of energy $E_{L\mathbf{k}}$ in the tip. According to Eqs. (S40) and (S41) and in accordance with the spin polarization of the YSR state, tunneling into the YSR state is due to spin-down electrons,

$$\begin{aligned} I|_+ &= \frac{2\pi e}{\hbar}\sum_{\mathbf{k}}|\langle \text{odd}; E_{Lk}|\psi^\dagger_{R\downarrow}(\mathbf{0})\left[-J^{(\text{d})}_{RL}(\mathbf{R})S + V^{(\text{h})}_{RL}(\mathbf{R})\right]\psi_{L\downarrow}(\mathbf{0})|\text{even}; \text{BCS}_L\rangle|^2\delta(eV - E_{Lk} - \epsilon_s) \\ &= \frac{2\pi e}{\hbar}|u_\epsilon(\mathbf{0})|^2\left[-J^{(\text{d})}_{RL}(\mathbf{R})S + V^{(\text{h})}_{RL}(\mathbf{R})\right]^2\sum_{\mathbf{k}}|\langle E_{Lk}|\psi_{L\downarrow}(\mathbf{0})|\text{BCS}_L\rangle|^2\delta(eV - E_{Lk} - \epsilon_s). \end{aligned} \tag{S43}$$

The sum over $\mathbf{k}$ can be identified with the superconducting density of states of the tip,

$$\nu_{L,\text{SC}}(E) = \nu_L\frac{|E|}{\sqrt{E^2 - \Delta^2}}\theta(\Delta - |E|), \tag{S44}$$

at energy $E = eV - \epsilon_s$, so that we obtain

$$I|_+ = \frac{2\pi e}{\hbar}|u_\epsilon(\mathbf{0})|^2\left[-J^{(\text{d})}_{RL}(\mathbf{R})S + V^{(\text{h})}_{RL}(\mathbf{R})\right]^2\nu_{L,\text{SC}}(eV - \epsilon_s). \tag{S45}$$

Importantly, the current involves interference between an exchange contribution associated with the molecular d orbital and a potential scattering contribution associated with the HOMO. The relative sign with which these contributions contribute directly reflects the fact that the tunneling current from tip to substrate is carried by spin-down electrons.

We will now see that the relative sign between these contributions is reversed at negative bias voltages, as in this case, current is carried by spin-up electrons. This can be seen from Eqs. (S40) and (S41). Physically, tunneling of an electron from the substrate into the tip breaks a Cooper pair in the even-parity ground state of the substrate. The spin-down electron of the Cooper pair occupies the YSR state, while the spin-up electron tunnels into the tip. This leads to

$$\begin{aligned} I|_- &= \frac{2\pi e}{\hbar}\sum_{\mathbf{k}}|\langle \text{odd}; E_{Lk}|\psi^\dagger_{L\uparrow}(\mathbf{0})\left[J^{(\text{d})}_{RL}(\mathbf{R})S + V^{(\text{h})}_{RL}(\mathbf{R})\right]\psi_{R\uparrow}(\mathbf{0})|\text{even}; \text{BCS}_L\rangle|^2\delta(-eV - E_{Lk} - \epsilon_s) \\ &= \frac{2\pi e}{\hbar}|v_\epsilon(\mathbf{0})|^2\left[J^{(\text{d})}_{RL}(\mathbf{R})S + V^{(\text{h})}_{RL}(\mathbf{R})\right]^2\nu_{L,\text{SC}}(e|V| - \epsilon_s) \end{aligned} \tag{S46}$$

for the YSR resonance negative bias.

Comparing Eqs. (S45) and (S46), we see that the relative signs of the exchange and potential-scattering contributions to the tunneling current differ between positive and negative bias voltages,

$$\left.\frac{\mathrm{d}I}{\mathrm{d}V}\right|_\pm \propto \left[\mp J^{(\text{d})}_{RL}(\mathbf{R})S + V^{(\text{h})}_{RL}(\mathbf{R})\right]^2, \tag{S47}$$

with the other contributions being essentially independent of the bias direction. Indeed, the electron and hole wavefunctions of the YSR state should be approximately equal, $|u_\epsilon(\mathbf{0})| \simeq |v_\epsilon(\mathbf{0})|$, due to the dominance of exchange coupling to the substrate implied by the well-developed Kondo correlations observed in experiment. We thus conclude that the YSR resonances should be symmetric between the bias directions when tunneling into the nodal plane of the HOMO, and have opposite asymmetries on the two sides of the nodal plane as a result of the sign change of $V^{(\text{h})}_{RL}(\mathbf{R})$.

Further comparison between theory and experiment

Experimentally, the Kondo and YSR asymmetries have different magnitudes. The experimental Kondo asymmetry, as parametrized by the angle ϕ, is small (compared to π), see Fig. 1e of the main text. In contrast, the YSR

asymmetries are of order unity, see Fig. 1f of the main text. This can be readily understood based on our theoretical results.

We first consider the Kondo resonance. According to Eqs. (S12) and (S15), the asymmetry emerges as follows. Tunneling between tip and magnetic orbital can proceed either directly [as described by the first term on the right hand side of Eq. (S12)] or indirectly via HOMO and substrate [as described by the second term on the right hand side of Eq. (S12)]. Indirect tunneling is a higher order process and should typically be smaller than the direct contribution. As the first contribution is real, while the second is imaginary (reflecting the continuum of states in the substrate), the phase ϕ is typically small in agreement with the experimental observation.

Next consider the YSR asymmetry. As we find in Eq. (S47), the asymmetry emerges from interference of two cotunneling paths. In one case, the electron cotunnels from the tip into the YSR state in the substrate via the magnetic orbital, in the other via the HOMO. Both paths give contributions of the same order, so that the YSR asymmetries are expected to be of order unity, again in agreement with our experimental data.

Using these results, we can further draw some conclusions about the spatial patterns of the Kondo and YSR resonances. First, we again consider the Kondo resonance whose spatial pattern of the amplitude of the Kondo resonance is shown in Fig. 2b. The smallness of the asymmetry parameter ϕ also implies that the amplitude of the Kondo resonance is dominated by t_d. Thus, its spatial pattern should be controlled by the magnetic orbital, with the HOMO only leading to small deviations. Consistent with this conclusion, the spatial pattern of the Kondo amplitude does not seem to resemble the experimental HOMO orbital shown in Fig. 3b. The HOMO only resembles the spatial pattern in the asymmetry of the Kondo resonance, consistent with Eq. (S12).

The spatial structure of the experimental YSR resonances shown in Figs. 2d,e shares gross features with the spatial pattern of the Kondo resonance. This should be expected as they also involve a large contribution due to cotunneling via the magnetic orbital. The HOMO resembles the spatial pattern in the asymmetry of the YSR resonances, consistent with Eq. (S47).

[1] M. Ruby, B. W. Heinrich, J. I. Pascual, and K. J. Franke, Phys. Rev. Lett. **114**, 157001 (2015).
[2] X. Chen, S. Lei, C. Lotze, C. Czekelius, B. Paulus, and K. J. Franke, J. Chem. Phys. **146**, 092316 (2017).
[3] G. Reecht, B. W. Heinrich, H. Bulou, F. Scheurer, L. Limot, and G. Schull, New J. Phys. **19**, 113033 (2017).
[4] P. Coleman and C. Pépin, Phys. Rev. B **68**, 220405 (2003).
[5] L. Farinacci, G. Ahmadi, G. Reecht, M. Ruby, N. Bogdanoff, O. Peters, B. W. Heinrich, F. von Oppen, and K. J. Franke, Phys. Rev. Lett. **121**, 196803 (2018).
[6] K. J. Franke, G. Schulze, and J. I. Pascual, Science **332**, 940 (2011).
[7] E. Minamitani, Y.-S. Fu, Q.-K. Xue, Y. Kim, and S. Watanabe, Phys. Rev. B **92**, 075144 (2015).
[8] V. Madhavan, W. Chen, T. Jamneala, M. F. Crommie, and N. S. Wingreen, Science **280**, 567 (1998).
[9] A. Schiller and S. Hershfield, Phys. Rev. B **61**, 9036 (2000).
[10] P. W. Anderson, Phys. Rev. Lett. **17**, 95 (1966).
[11] S. Frank and D. Jacob, Phys. Rev. B **92**, 235127 (2015).
[12] O. Újsághy, J. Kroha, L. Szunyogh, and A. Zawadowski, Phys. Rev. Lett. **85**, 2557 (2000).
[13] H. O. Frota, Phys. Rev. B **45**, 1096 (1992).
[14] M. Ruby, F. Pientka, Y. Peng, F. von Oppen, B. W. Heinrich, and K. J. Franke, Phys. Rev. Lett. **115**, 087001 (2015).